Int. J. Solids Structures Vol. 27, No. 6, pp. 699–711, 1991
Printed in Great Britain.

0020–7683/91 $3.00 + .00
Pergamon Press plc

TRANSIENT ACOUSTIC SCATTERING BY FLUID-LOADED ELASTIC SHELLS

G. C. GAUNAURD and W. WERTMAN
Naval Surface Warfare Center, White Oak Laboratory, Silver Spring, MD 20903-5000, U.S.A.

(*Received* 28 *December* 1989; *in revised form* 20 *April* 1990)

Abstract—We study the general scattering interaction of acoustic pulses of arbitrary shape and duration with a submerged elastic spherical shell. We first obtain the backscattering or sonar cross-section (SCS) of such a target and analyze the resonance features that are present within its resonance region. The elastic composition of the shell makes the resonance features become very prominent in a very wide band. Transient echoes from submerged shells are related to poles of the scattering amplitude and to their associated residues in the complex frequency plane. We show by exact Fourier synthesis that the individual resonances associated with each pole (i.e., eigenfrequencies) can be obtained and studied one at a time, provided we use long illuminating pulses, since these excite transients at their carrier frequencies that ring and decay. Of greater practical importance is the use of short pulses, not only because these are the most frequently used by sonars, but because they are shown here to produce backscattered pulses with spectra that replicate the entire set of features in the SCS of the shell. This replication of the SCS occurs in bands that have widths directly proportional to their energy and their carrier frequency, x_0. Our computational methodology can handle pulses of any duration, shape, and any conceivable spectra, as well as lossless or lossy fluid-loaded shells, either single or multi-layered. We can predict the returns in all instances. For long insonifying pulses, the backscattered echoes exhibit a double transient nature when x_0 coincides with any shell resonance. The successive tail bursts that follow the specular part of the return in the time domain not only are seen to decrease in amplitude, but the decrease occurs in distinct discrete jumps. We predict the backscattered echoes for various types of pulses, carrier frequencies, bands, shapes and durations and we display the results in the (non-dimensional) time and frequency domains, while giving the appropriate physical interpretations of the results in all instances.

1. INTRODUCTION

Numerous works have studied the scattering of acoustic continuous waves (c.w.) by elastic shells submerged in fluids. These studies have all been motivated by a desire to describe and model the interaction of active sonars at sea with the submerged shells of their interest. Since the volume of (open) publications from East to West on this subject is literally gargantuan, it will only be possible to mention a few in this brief introduction.

Among the earliest works dealing with the spherical geometry and c.w. incidences are the articles of Junger (1951), Junger and Feit (1969a), Feit and Junger (1969), and Goodman and Stern (1962). Many other authors have also left their imprint, such as Hickling (1964), Sergeev (1985), and Fender (1972). Much of this work has been incorporated into books and monographs such as Junger and Feit (1972) and Veksler (1982, 1984).

The interaction of an active sonar with a scatterer is essentially a transient process. Most sonars purposely use either long or short pulses, often of strange shapes and various frequencies. To analytically or numerically deal with pulses as interrogating waveforms is far more complicated. A number of works have dealt with the fundamentals of this more general case such as the books of Nigul (1974), Friedlander (1958), and Metsaveer *et al.* (1979), as well as the articles of Weyker and Dudley (1987), and Kraus and Kalnins (1965). The exact analysis of the scattering of various types of incident pulses by a submerged spherical shell seems to have been ignored up to the present. We present here a detailed study of the scattering interaction of pulses of various shapes and durations with a fluid-loaded elastic spherical shell, and show the advantage/disadvantage in the use of various pulse-shapes and pulse-durations. Although similar situations have been preliminarily treated in a recent conference by Gaunaurd (1990), and by Werby (1989), for the case of submerged shells near an environmental interface, we will not introduce such added complication here, and leave it for a separate study (Gaunaurd and Werby, unpublished results).

We draw some comparisons to the radar literature of over three decades ago, particularly to the articles of Kennaugh and Cosgriff (1958), and Kennaugh and Moffatt (1965), where analogous electromagnetic situations were analyzed. The code we have developed to produce our calculations can generate predictions for the backscattered returns for elastic as well as lossy (i.e., viscoelastic or viscoelastically-coated) shells, for any type of incident pulse, having any spectrum, and in any frequency band. We display numerous results and give their physical interpretation.

2. CLASSICAL SOLUTION IN THE STEADY-STATE (c.w.) CASE

Consider a plane sound wave incident on a spherical shell of outer radius a and inner radius b. This incident wave is:

$$p_{\text{inc}}(r, \theta, t) = p_0 \exp\left(i(k_1 r \cos\theta - \omega t)\right). \tag{1}$$

The scattered pressure field is

$$p_{\text{sc}}(r, \theta, t) = p_0 \, e^{-i\omega t} \sum_{n=0}^{\infty} i^n (2n+1) T_n(x) P_n(\cos\theta) h_n^{(1)}(x), \tag{2}$$

where $x \equiv k_1 a$ and the incidence is on the South pole of the sphere. The total pressure field is the sum of the two, namely

$$p_t(r, \theta\, t) = p_0 \, e^{-i\omega t} \sum_{n=0}^{\infty} i^n (2n+1) P_n(\cos\theta)[j_n(k_1 r) + T_n(x) h_n^{(1)}(k_1 r)]. \tag{3}$$

For an elastic shell filled with air and immersed in water, the coefficients $T_n(x)$ are determined from the boundary conditions and they turn out to be given by ratios of two 6×6 determinants, namely

$$T_n = \frac{B_n(x)}{D_n(x)}$$

$$= -\begin{bmatrix} Red_{11} & d_{12} & d_{13} & d_{14} & d_{15} & 0 \\ Red_{21} & d_{22} & d_{23} & d_{24} & d_{25} & 0 \\ 0 & d_{32} & d_{33} & d_{34} & d_{35} & 0 \\ 0 & d_{42} & d_{43} & d_{44} & d_{45} & d_{46} \\ 0 & d_{52} & d_{53} & d_{54} & d_{55} & d_{56} \\ 0 & d_{62} & d_{63} & d_{64} & d_{65} & 0 \end{bmatrix} \Bigg/ \begin{bmatrix} d_{11} & d_{12} & d_{13} & d_{14} & d_{15} & 0 \\ d_{21} & d_{22} & d_{23} & d_{24} & d_{25} & 0 \\ 0 & d_{32} & d_{33} & d_{34} & d_{35} & 0 \\ 0 & d_{42} & d_{43} & d_{44} & d_{45} & d_{46} \\ 0 & d_{52} & d_{53} & d_{54} & d_{55} & d_{56} \\ 0 & d_{62} & d_{63} & d_{64} & d_{65} & 0 \end{bmatrix} \tag{4}$$

where the elements d_{ij} are all known and were given elsewhere (cf. Ayres *et al.*, 1987).

In the far-field, $k_1 r \gg 1$, the asymptotic expansion for the spherical Hankel function, given in Arfken (1966), is valid, and the scattered pressure can be expressed as:

$$p_{\text{sc}}(r, \theta, t) \xrightarrow[kr \gg 1]{} \frac{p_0 a}{2r} \exp\left[i(k_1 r - \omega t)\right] \cdot \left[\frac{2}{a} f_\infty(\theta, x)\right] \tag{5}$$

where the scattering pattern in the last bracket is

$$\frac{2}{a} f_\infty(\theta, x) = \frac{2}{ix} \sum_{n=0}^{\infty} (2n+1) T_n(x) P_n(\cos\theta). \tag{6}$$

In the backscattering direction $\theta = \pi$, the sonar cross-section (SCS) is

$$\frac{\sigma_B}{\pi a^2} = \left|\frac{2}{a} f_\infty(\pi, x)\right|^2 = \left|\frac{2}{ix} \sum_{n=0}^{\infty} (-1)^n T_n(x)(2n+1)\right|^2. \tag{7}$$

This concludes this synopsis of the backscattering problem in the c.w. case, as was found previously in Ayres *et al.* (1987) (see Appendix).

3. THE TRANSIENT SOLUTION FOR PULSED INCIDENCES

From eqns (5) and (6), the scattered pressure field can be expressed as

$$p_{sc}(r, x, \tau') = \frac{p_0}{r} e^{-ix\tau'} \frac{a}{2}\left[\sum_{n=0}^{\infty} (-1)^n (2n+1) T_n(x)\right] \tag{8}$$

where $\tau' = (ct-r)/a$. Consider a Fourier transform pair in the canonical variables x and τ', namely

$$G(x) = \int_{-\infty}^{+\infty} g(\tau') e^{ix\tau'} d\tau' \quad \text{and} \quad g(\tau') = \frac{1}{2\pi} \int_{-\infty}^{+\infty} G(x') e^{-ix'\tau'} dx'. \tag{9}$$

It was repeatedly shown by Gaunaurd and Ueberall (1985) and Ueberall and Gaunaurd (1984) that to go from steady-state [eqn (8)] to transient solutions, all that one needs to do is to replace the exponential $p_0 e^{-ix\tau'}$ by the right-hand side of the second of eqns (9), namely

$$p_0 e^{-ix\tau'} \longleftrightarrow \frac{1}{2\pi} \int_{-\infty}^{+\infty} G(x') e^{-ix'\tau'} dx'. \tag{10}$$

It is obvious that if $G(x') = 2\pi p_0 \delta(x-x')$, then eqn (10) is an identity. With this simple replacement, eqn (8) becomes:

$$p_{sc}(r, x, \tau') = \frac{a}{2} \sum_{n=0}^{\infty} \frac{(2n+1)}{r} \frac{(-1)^n}{ix} \int_{-\infty}^{+\infty} G(x') T_n(x') e^{-ix'\tau'} \frac{dx'}{x'}. \tag{11}$$

Equation (11) is the generalization of eqn (8), now for pulsed incidences. Using the definition of the backscattered form-function in eqn (7), namely

$$f_\infty(\pi, x) = \frac{a}{ix} \sum_{n=0}^{\infty} (-1)^n (2n+1) T_n(x) \tag{12}$$

in eqn (11) yields

$$r p_{sc}(\pi, \tau') = \frac{1}{2\pi} \int_{-\infty}^{+\infty} [f_\infty(\pi, x') G(x')] e^{-ix'\tau'} dx'. \tag{13}$$

This means that the scattered pulse in the τ'-domain is the inverse Fourier transform of the single-frequency response [namely the form-function $f_\infty(\tau, x')$] weighted by the spectrum of the incident pulse. It is possible to apply input/output concepts of linear systems theory to scattering situations. Defining the transform pair:

$$f_x(\hat{n}, x) = \int_{-\infty}^{+\infty} \bar{f}_x(\hat{n}, \tau)\, e^{-ix\tau}\, d\tau \tag{14}$$

$$\bar{f}_x(\hat{n}, \tau) = \frac{1}{2\pi} \int_{-\infty}^{+\infty} (\hat{n}, x')\, e^{-ix'\tau}\, dx' \tag{15}$$

valid in any direction $\hat{n}$, then eqn (13) can be alternatively expressed in the equivalent convolution form:

$$rp_{sc}(\pi, \tau') = \int_{-\infty}^{+\infty} g(\tau - \tau') \bar{f}_x(\pi, \tau)\, d\tau, \tag{16}$$

which states that the scattered pulse in the τ'-domain is the convolution of the incident pulse $g(\tau)$ and the scattered waveform for an impulsive source, also called the impulse response in the τ'-domain. These linear system concepts were introduced into the (radar) *scattering* literature by Kennaugh and Cosgriff (1958), and by Kennaugh and Moffatt (1965), and these works presented useful approximations to generate estimates of the scattered pulses. In what follows, we have computed our results by exact Fourier synthesis and have not used the mentioned approximations. It is clear that if we substitute $G(x') = 2\pi p_0 \delta(x - x')$ into the transient solution in eqn (13), we then recover the steady-state solution in eqn (5) for c.w. incidences.

The form of eqn (13) most suitable for computations is:

$$rp_{sc}(\pi, \tau') = \sum_{n=0}^{\infty} H_n(\tau') \tag{17}$$

where

$$H_n(\tau') = \frac{1}{2\pi} \int_{-\infty}^{+\infty} [G(x') f_n(\pi, x')]\, e^{-ix'\tau'}\, dx' \tag{18}$$

and

$$f_n(\pi, x') = \frac{a}{ix'} (-1)^n (2n+1) T_n(x') \tag{19}$$

where the $T_n(x)$ are the determinant ratios in eqn (4), and where we have defined:

$$f_\infty(\pi, x') \equiv \sum_{n=0}^{\infty} f_n(\pi, x'). \tag{20}$$

We now illustrate these ideas with numerical calculations pertaining to an air-filled steel shell submerged in water under insonification by various types of pulses.

4. TYPES OF PULSES USED

The idea is to use any arbitrary interrogating short or long pulse. A few examples are illustrated below.

Type 1: constant pulse of duration τ^*

This is given by

$$g_1(\tau) = \begin{cases} A & 0 \leqslant \tau \leqslant \tau^* \\ 0 & \text{elsewhere} \end{cases} \tag{21}$$

and the spectrum is

$$G_1(x) = A\tau^* \cdot \frac{\sin(x\tau^*/2)}{(x\tau^*/2)} e^{ix\tau^*/2}. \tag{22}$$

Type 2: damped cosinusoid starting at $\tau = 0$

This is given by

$$g_2(\tau) = \begin{cases} A e^{-b\tau} \cos x_0\tau & \tau > 0 \\ 0 & \tau < 0 \end{cases} \tag{23}$$

and its spectrum is

$$G_2(x) = A \frac{b(b^2 + x^2 + x_0^2) + ix(b^2 + x^2 - x_0^2)}{(b^2 + x_0^2 - x^2)^2 + 4b^2x^2}. \tag{24}$$

Type 3: sinusoid of duration τ^*

$$g_3(\tau) = \begin{cases} \sin x_0\tau & 0 \leqslant \tau \leqslant \tau^* \\ 0 & \text{elsewhere.} \end{cases} \tag{25}$$

The sinusoid has N cycles in the duration τ^*, namely $\tau^* = 2\pi N/x_0$. Its spectrum is

$$G_3(x) = \frac{1 - e^{i(x+x_0)\tau^*}}{2(x+x_0)} - \frac{1 - e^{i(x-x_0)\tau^*}}{2(x-x_0)}. \tag{26}$$

Any other conceivable pulse can be handled numerically by means of available fast Fourier transform (FFT) software packages discussed in volumes such as Press *et al.* (1986). The spectra given above [cf. eqns (22), (24) and (26)] are found by direct evaluation of eqn (9a) or from available tables such as Campbell and Foster's (1948), or Champeney's (1973).

5. NUMERICAL RESULTS AND DISCUSSION

A plane sound-wave is incident on the South pole of a spherical stainless-steel shell of outer radius a and inner radius b. The shell has dimensions $a = 505$ cm, $b = 500$ cm, and therefore, $h \equiv 1 - b/a \cong 1\%$. The shell is air-filled and it is submerged in water. The material parameters of the shell and its surrounding fluids are given in Table 1. To relate E to ν to the shear and dilatational wavespeeds we use:

Table 1. Material parameters of the shell and the fluids

	Density ρ (g cm^{-3})	Dilatational speed c_d (cm s^{-1})	Shear speed c_s (cm s^{-1})	Young's modulus E (dyne cm^{-2})	Poisson's ratio, ν
Stainless steel	7.9	5.78×10^5	3.09×10^5	19.6×10^{11}	0.3
Water	1.0	1.5×10^5	0	—	—
Air	0.0012	0.344×10^5	0	—	—

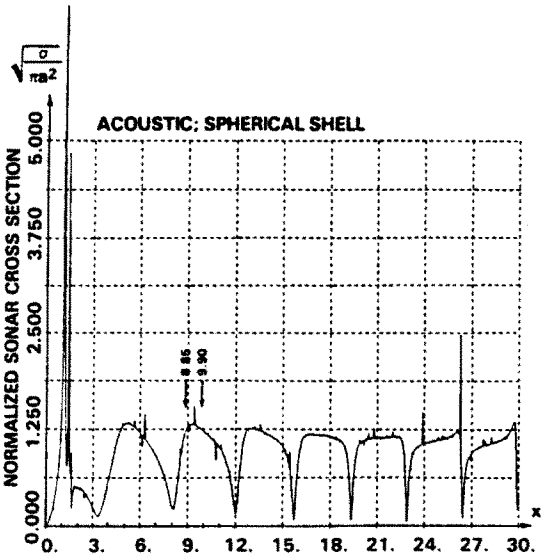

Fig. 1. Backscattering or sonar cross-section (SCS) of an air-filled, stainless steel spherical shell immersed in water versus non-dimensional frequency x ($= k_1 a$). The material properties are given in Table 1. The shell thickness is $h \cong 1\%$. The arrows indicate (low-frequency) spectral locations coinciding or not with a shell resonance.

$$E = \frac{\rho c_s^2(4c_s^2 - 3c_d^2)}{c_s^2 - c_d^2} \quad \text{and} \quad \nu = \frac{2c_s^2 - c_d^2}{2(c_s^2 - c_d^2)},$$

or inverting

$$c_s = \sqrt{\frac{E}{2\rho(1+\nu)}} \quad \text{and} \quad c_d = c_s\sqrt{\frac{2(1-\nu)}{1-2\nu}}.$$

In the earlier work of Gaunaurd and Werby (1987), slightly lighter steel, and also lighter aluminum and tungsten carbide (WC), were used.

Figure 1 shows the (normalized) sonar cross-section (SCS) of the shell as computed by the classical expression, eqn (7), for the case of c.w. incidences. The frequency band displayed is: $0 \leqslant x \equiv ka \leqslant 30$. We had found similar SCS for similar shells in much wider ($0 \leqslant x \leqslant 200$) bands. Our main interest is now for: $x \leqslant 10$. We note a peak at $x_0 = 8.85$ and a plateau at $x_0 \cong 9.90$, among many others. The methodology of the resonance scattering theory (RST) as applied to spherical shells (see, for example, Gaunaurd and Kalnins, 1982) has shown that subtraction of the rigid or soft "backgrounds" from the elastic response in Fig. 1 isolates the resonances. These backgrounds are displayed in Fig. 2a in the same band, for illustration purposes. For the present shell in this band, the rigid background seems to be the proper background to suppress in order to extract the resonances, as discussed by Gaunaurd and Werby (1986). Except for a strong resonance in the interval $1 \leqslant x \leqslant 3$ that manifests itself in a sequence of contiguous peaks, the SCS in Fig. 1 exhibits the usual pattern of inverted Us. The resonance peaks/dips appear superimposed on the background which, as can be seen in Fig. 1, is mostly flat with small deviations around an ordinate value of unity. Thus, for the most part, the frequency response is that of an impenetrable scatterer. Sound penetration into the structure takes place only through narrow spectral windows centered at the shell resonances. Figure 2b shows the result of subtracting the rigid background from the elastic response in Fig. 1.

Figure 3 shows the spectrum $G_2(x)$ of a Type 2 pulse [cf., eqn (24)] displayed in absolute value vs frequency in the case of a small amount of damping (namely $h \cong x_0/20$) and a carrier frequency $x_0 \sim 11$. These values are arbitrary. The location of the spectral peaks occurs at the value of carrier frequency x_0.

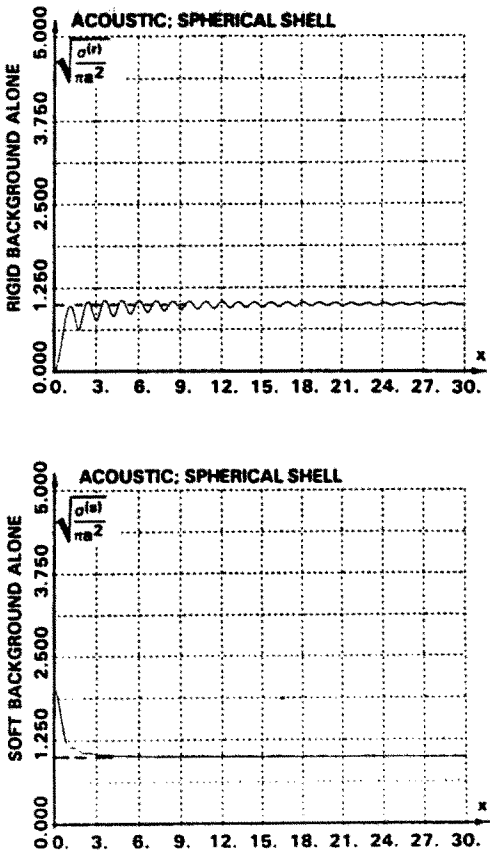

Fig. 2(a). The rigid (top) and soft (bottom) backgrounds associated with the same shell, in the same frequency band: $0 \leqslant x \leqslant 30$. These are the spectral responses of impenetrable spheres of the same size but of opposite and extreme compositions.

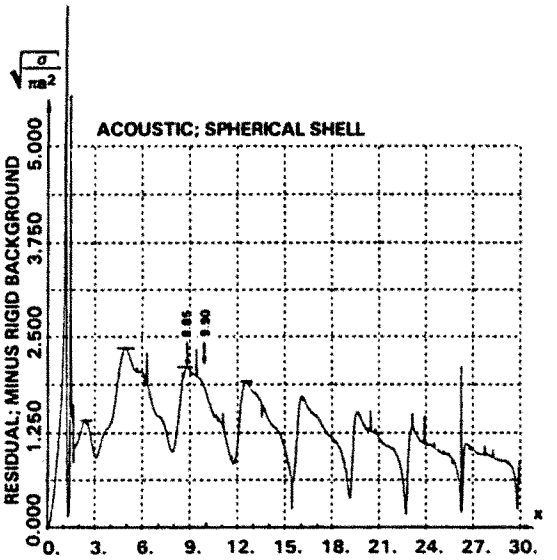

Fig. 2(b). Residual response obtained by subtracting the rigid background (Fig. 2a, top) from the elastic response (in Fig. 1), in the manner of the RST. Resonance peaks are isolated in this fashion. We selected the third such peak (at 8.85) as our basic resonance.

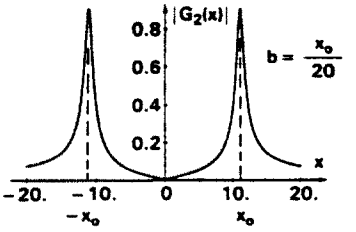

Fig. 3. Spectrum of an incident Type 2 pulse with carrier frequency x_0 and damping constant $b = x_0/20$. The spectrum is complex and is displayed in modulus vs x. The peak occurs at $x = x_0$.

Figure 4 shows short (top) and long (bottom) *incident* Type 3 pulses (cf. left column) and their spectra (cf. right column) as given by eqns (25) and (26), respectively. In both cases the carrier frequency is fixed at $x_0 = 8.85$, which coincides with a resonance peak in Figs 1 and 2b. The short pulse has (non-dimensional) duration $\tau^* = 1$, and for this carrier frequency it has $N = 1.4$ cycles. The long pulse has $N = 20$ cycles and duration $\tau^* = 14.2$. The peak of the spectrum always appears at the carrier frequency x_0 and there are an infinity of side-lobes on both sides. The zero-crossings are x_0/N apart in the spectrum. These complex spectra are displayed in absolute values.

The *scattered* pulses are much harder to compute. We use either eqn (13) or eqns (17)–(20). Figure 5 shows the result of the calculation for the backscattered pulse (left column) which results when a short incident pulse hits the shell (cf. Fig. 4a). The carrier frequency is $x_0 = 8.85$ (top) and $x_0 = 9.90$ (bottom). The backscattered pulse (left column) shows the initial replica of the incident pulse, followed by a long tail. The bottom graphs correspond to the case where x_0 coincides with a plateau of Fig. 1. Hence, here the carrier frequency coincides, or not, with a shell resonance. The main advantage of using short pulses is that their backscattered spectra at resonance (upper right) reproduce the features (marked by

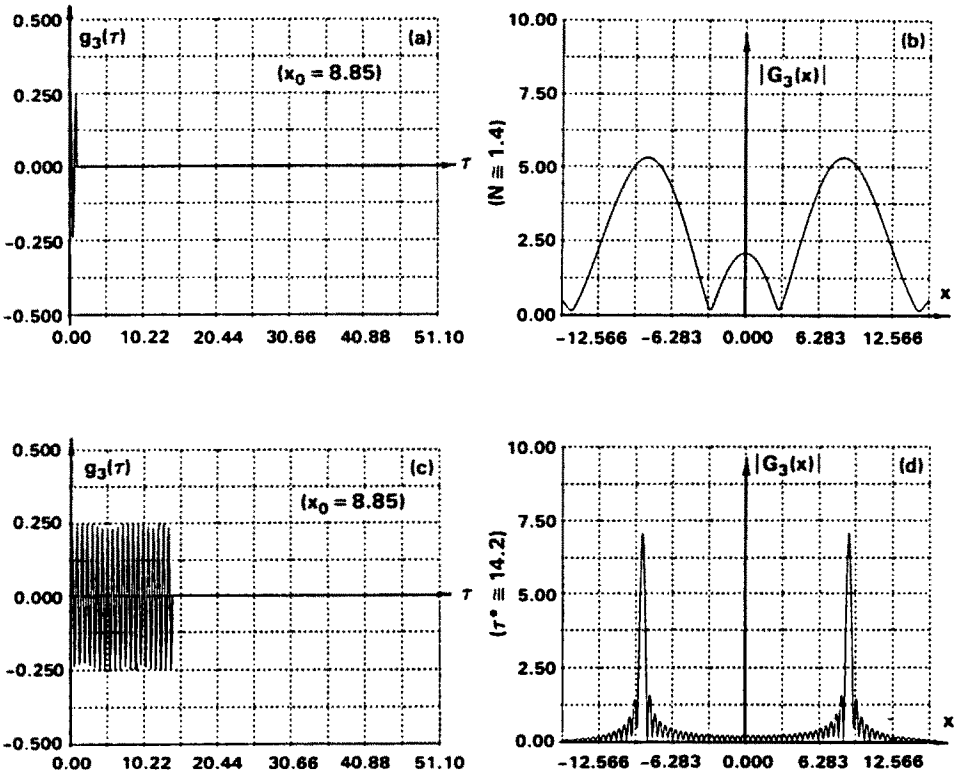

Fig. 4. Short (top) and long (bottom) *incident* Type 3 pulses (left column) of carrier frequency $x_0 = 8.85$. The pulse duration of the short one is $\tau^* = 1$ and the number of cycles of the long one is $N = 20$. Their spectra are shown in modulus in the right column. They show peaks at the carrier frequency x_0 with $N = \infty$ lobes at both sides.

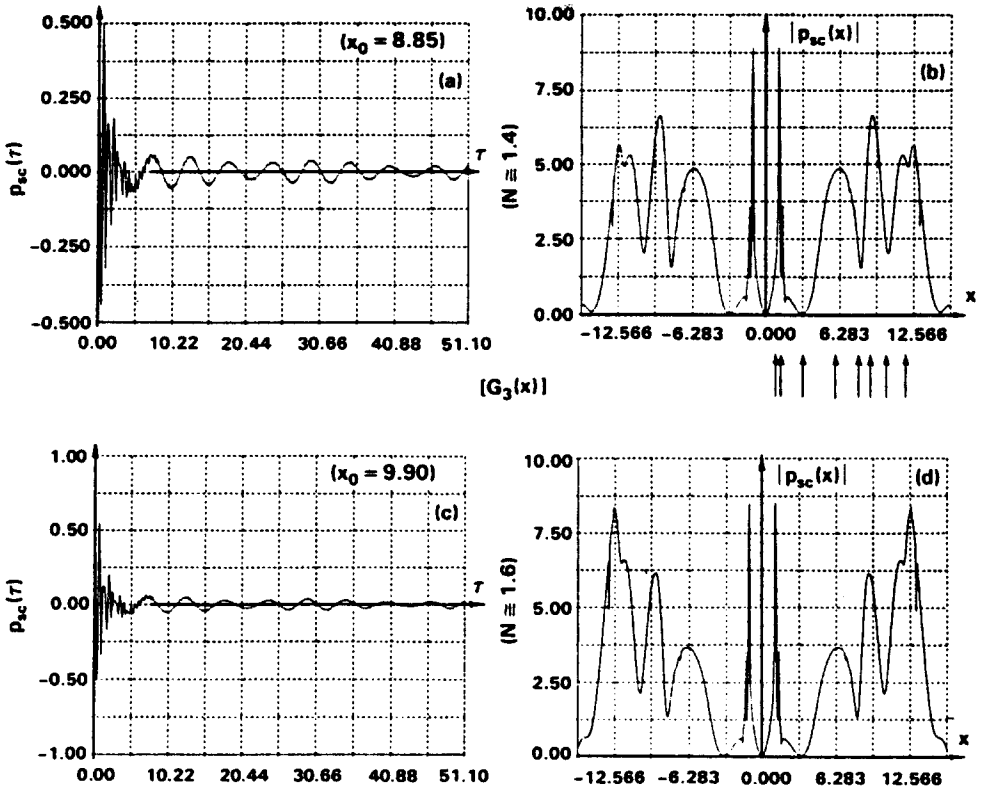

Fig. 5. Backscattering pulses resulting when *short* incident pulses of carrier frequency $x_0 = 8.85$ (top) and $x_0 = 9.90$ (bottom) are returned by the shell. Their respective rectified spectra are displayed in the right column. In the upper (lower) case, the carrier frequency coincides (or not) with a shell resonance. The left column exhibits the amplitude decrease of the successive tail bursts in discrete steps. The right column shows the replication, up to $x \sim x_0^*$ of the SCS we saw in Fig. 1, in a more evident fashion in the upper right plot.

arrows) of the SCS as they appear in Fig. 1, at least up to the chosen value of x_0, with a fast decay afterwards. In the (non-dimensional) τ-domain, the tail of the scattered pulse consists of a sequence of bursts each a few cycles long and of progressively decreasing amplitudes which are seen to decrease *in discrete steps* as illustrate in Fig. 5 (left column).

These trailing bursts are the creeping-wave components of the returned echo—modified by the fact that the target is now elastic rather than impenetrable—as they have been analyzed by Gaunaurd and Ueberal (1985) and Ueberal and Gaunaurd (1984). The spectra in the right column are obtained by means of the FFT package given by Press *et al.* (1986). Thus, a short incident sinusoidal pulse excites all the resonances in the shell and after scattering, it yields a replica of the shell's SCS up to frequencies slightly above the value of the carrier frequency. The replica is more accurate when the carrier frequency coincides with a target resonance (upper right) than when it does not (bottom right).

The result of using Type 1 and Type 2 pulses is illustrated in the top and bottom halves of Fig. 6, respectively. The tails of the backscattered pulses displayed the same sequence of bursts of decreasing amplitude, all with the amplitudes decreasing in *discrete steps or jumps*. The spectrum in the bottom right graph shows a peak at the carrier frequency, which in that case was chosen to be $x_0 = 8.85$. The upper right plot is for a pulse without carrier frequency, and that explains the poorly informative results it yields. These graphs all display the real part of the scattered pressure field. The imaginary part vanishes identically in all instances.

Figure 7 displays the backscattered pulses resulting when long Type 3 pulses of $N = 20$ cycles are incident on the shell. These scattered pulses exhibit an initial (specular) portion followed by a succession of bursts of decreasing amplitude which (again) are seen to decrease in *discrete steps*. We note in these cases that both the incident and scattered pulses

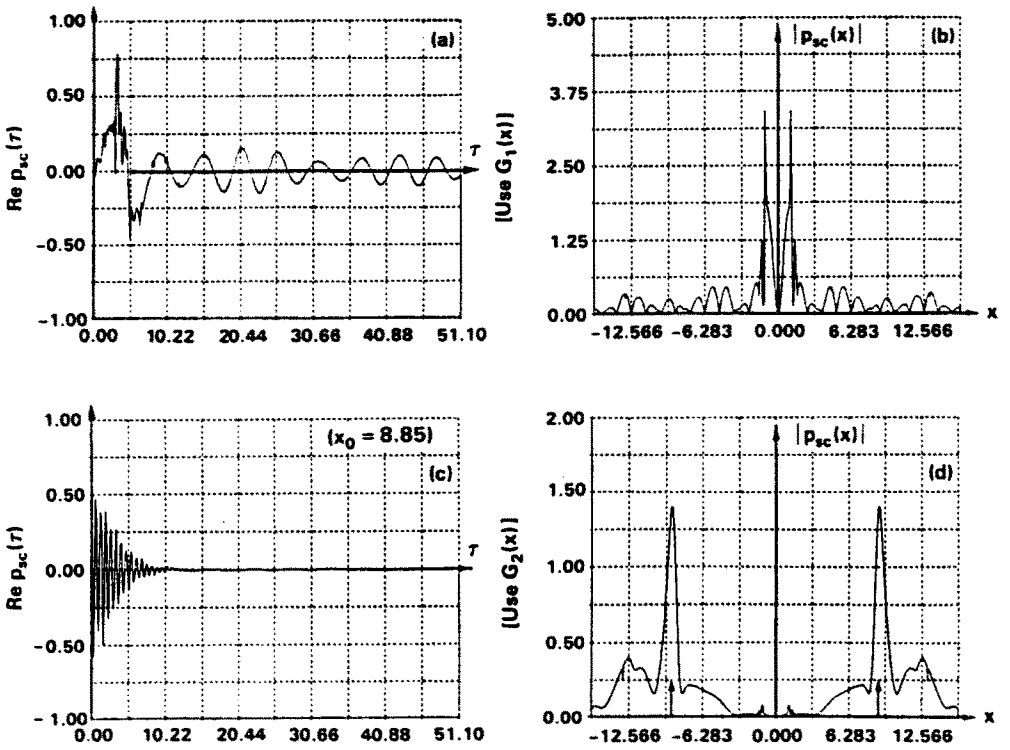

Fig. 6. Backscattered pulses resulting when incident Type 1 (top) and Type 2 (bottom) pulses are returned by the shell. Their respective spectra are shown rectified in the right column. The bottom right spectrum exhibits a peak at $x = x_0 = 8.85$, not present in the upper right plot since Type 1 pulses have no carrier frequency. The τ-domain plots (left) still show the amplitude decrease of the tail bursts in discrete steps.

have duration $\tau^* \cong 14.2$ when $x_0 = 8.85$ (at resonance), and duration $\tau^* \cong 12.7$ when $x_0 = 9.90$ (away from resonance), as we can verify in Figs 4 and 7. The spectra in the right column of Fig. 7 have strong peaks at the carrier frequency and smaller values everywhere else. A long pulse of carrier frequency x_0 has most of its spectral response at that frequency, as we see in Fig. 4. This continues to be the case after scattering as can be verified in Fig. 7. The spectral differences between the incident and scattered pulses appear mostly in the side-lobes, and are relatively small (cf. Figs 4 and 7). This non-uniformity of the side-lobes in the scattered spectra (cf. Fig. 7, right column) is the cause of the long tail behind the specular portion of the response in the τ-domain. We further note that away from any resonance (bottom plots, $x_0 = 9.90$) the specular portion of the return is an accurate replica of the incident pulse. However, near a shell resonance (at $x_0 = 8.85$, upper plots) a constriction or narrowing appears in the middle of the specular portion of the return. This constriction is an indication of the double transient nature of the response, and of the fact that x_0 is then coinciding with one of the shell resonances.

6. PHYSICAL INTERPRETATION AND CONCLUSIONS

We have generated the exact scattering solution for several cases in which either long or short incident pulses of various shapes are scattered by elastic spherical shells in water. These transient interactions are fundamental in practice since sonar interrogration is essentially a transient process.

If long sinusoidal pulses are used as incident waveforms on submerged shells, we have actually demonstrated by Fourier synthesis that when the carrier frequency of the pulse coincides with any of the shell resonances, the spectrum of the resulting scattered pulse basically consists of a large resonance peak that is created precisely at that frequency, that later rings and decays. This seems to be in keeping with the predictions of a radar scattering

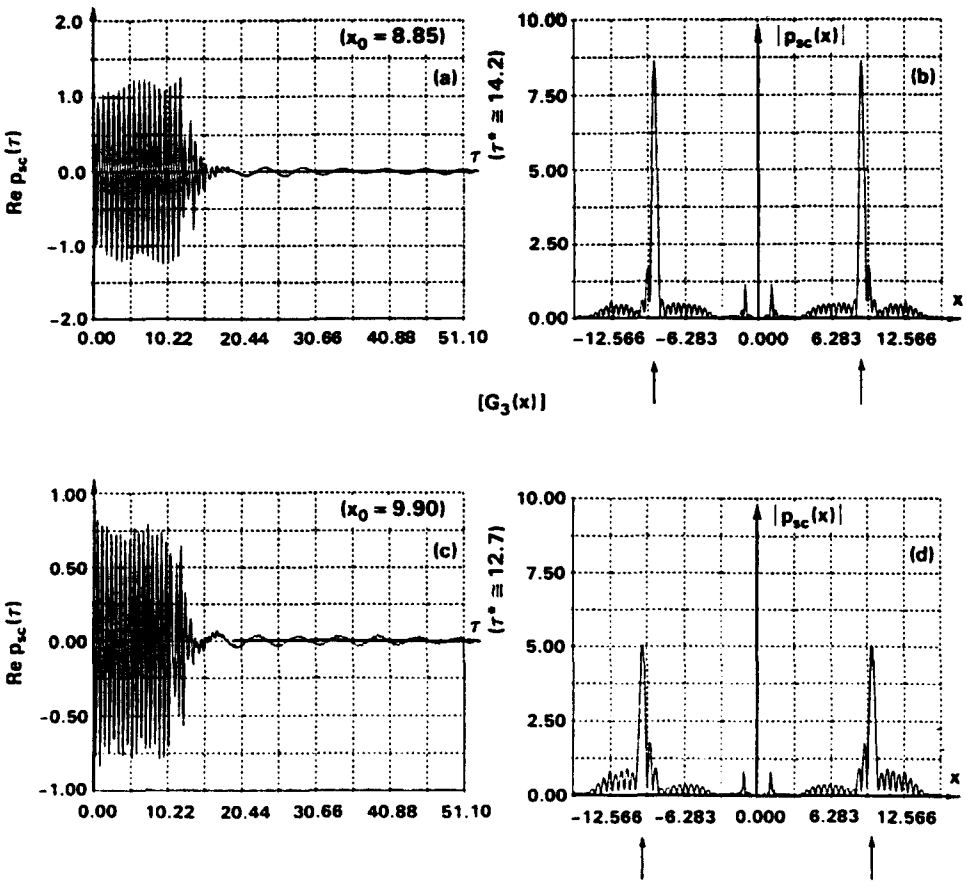

Fig. 7. Backscattered pulses resulting when *long* incident pulses of carrier frequency $x_0 = 8.85$ (top, at resonance) and $x_0 = 9.90$ (bottom, away from resonance) are returned by the shell. Their respective rectified spectra are displayed in the right column. The τ-domain plots (left) show the amplitude decrease of the tail bursts which occurs in discrete steps, and also the constriction in the middle of the specular part of the return that developes (top) when x_0 coincides with a shell resonance. The spectra (right column) show peaks at the respective carrier frequencies, with sets of non-uniform minor lobes on both sides. This shows that long incident pulses (as in Fig. 4, bottom) have *backscattered* returns with spectra having *main* contributions just at the carrier frequency, as postulated in radar cases by the Singularity Expansion Method.

approach known as the Singularity Expansion Method developed by Baum (1976), which associates individual (ringing) pole-resonances with damped sinusoids. It then follows that individual pole-resonances can be identified one by one from the observation of their ringing. If the carrier frequency of the incident pulse does not coincide with any of the shell resonances, then no ringing develops, and no identification is possible.

For the more important case of the short incident pulses, it turns out that the back-scattered (transient) response contains all the resonance features of the SCS (or steady-state response, or single frequency response) for the c.w. case. We have recovered these features by actual Fourier synthesis in frequency bands that go slightly beyond the value of the carrier frequency. This is the main advantage of using short pulses of high energy content. A short pulse has a broad spectrum (cf. Heisenberg's Uncertainty Principle) that can excite many resonances at the same time, and their contributions superimpose in the scattered return forming the shell's SCS.

We underline here that although the shell used in our analysis was purely elastic, it could have had viscoelastic losses (namely sound-absorption capability). That would have meant that the shear and dilatational wavenumbers k_{d_2} and k_{ℓ_2} in the shell could have been complex rather than real. Our computational code is equally effective in this viscoelastic case, and also when the shell is covered with a sound-absorbing layer, as discussed by Gaunaurd and Kalnins (1982).

The simple two-line derivation of eqn (11) that we gave rests on the observation made earlier (see, for example, Ueberal and Gaunaurd, 1984) that the correct result follows with the replacement we have shown in eqn (10). We repeat that the resonance features in an SCS from a penetrable (i.e., elastic) body can be isolated by a process of background suppression (cf. Fig. 2b) that we have repeatedly obtained and explained (see, for example, the review of Gaunaurd, 1989), which amounts to subtracting from each mode $f_n(\pi, x)$ the corresponding contribution from an identical scatterer of impenetrable composition. The resonance "lines" that are thus isolated constitute the target's *spectrogram*. An alternative procedure that does not require background subtraction is to determine the poles of the scattering amplitude by solving the corresponding eigenfrequency condition. In the present case, the poles are the zeros in the denominator of the coefficients $T_n(x)$ [the zeros of $D_n(x)$ in eqn (4)]. These poles split into two great families, as found by Gaunaurd (1987). One family, due to the scatterer's *shape*, is almost indistinguishable from the poles of a rigid sphere, which are given by the roots of $h_n^{(1)'}(x) = 0$ in the complex x-plane. We have computed and displayed all these poles elsewhere (for example, in the review by Gaunaurd, 1989b). The other family appears just below the real axis, in the lower half of the complex x-plane. This family is purely due to target *composition* or elastic penetrability. These two clearly distinguishable families of poles separate the effects of shape and composition. Each sub-family within each of these two great families of poles can be used to generate dispersion plots for the phase or group velocities or attenuations of the surface waves excited within the shell material, and of the various creeping-waves revolving around the shell in the outer medium. The procedure rests on very simple formulas given in the mentioned review. A spectral resonance (or "line") is associated with the real part of the corresponding pole-position, and its "width" is associated with the imaginary part. The larger the (negative) ordinate of a pole is, the more attenuated will be the surface wave associated with that pole. The poles closest to the real axis (such as the *composition* poles) are the ones that have the strongest influence. More distant poles have more attenuated contributions.

The "double transient" shape of backscattered pulses (cf. Fig. 7) has been observed by Gaunaurd and Tsui (1988) and Tsui *et al.* (1988), and others, in experiments dealing with cylindrical shells. This peculiar pulse shape exhibits a narrow region—the forced vibration region—in the middle of the initial or specular part of the return, whenever x_0 coincides with a shell resonance. Away from any resonance such a constriction is not formed or seen. This behavior at resonance was explained on the basis of the response of a simple harmonic oscillator(!). As the initial transient caused by the interaction of the shell with the leading edge of the pulse dies out, a steady-state region develops that is later interrupted as the tail edge of the pulse interacts again with the shell as it goes by. This final interaction with the tail-end produces the second transient, which is followed by the final ringing and decay of the response. Sampling the backscattered pulses within the constriction (i.e., in the forced-vibration region) yields a complicated pattern because many harmonics interact there (see Gaunaurd and Tsui, 1988) to produce the SCS. Sampling past the second transient region, just as the ringing starts, *isolates* the single resonance component that is decaying. This behavior at resonance can be exploited to extract information about the penetrable nature of the shell, which serves to characterize it uniquely. This target-identification capability is not possible if x_0 does not coincide with any of the shell resonances as manifested in its SCS. We conclude by stating that the code we have developed can handle any type of incident pulse, in any frequency band, for lossless or lossy shells. Portions of this work were presented at an international meeting (Strifors and Gaunaurd, 1989).

REFERENCES

Arfken, G. (1966). *Mathematical Methods for Physicists*, eqns 11.159. Academic Press, New York.

Ayres, V. M., *et al.* (1987). The effects of Lamb waves on the sonar cross-sections of elastic spherical shells. *Int. J. Solids Structures* **23**, 937–946.

Baum, C. (1976). The singularity expansion method. In *Transients in Electromagnetic Fields* (Edited by L. B. Felsen), pp. 129–179. Springer, Berlin.

Campbell, G. and Foster, R. (1948). *Fourier Integrals for Practical Applications*. Academic Press, New York.

Champeney, D. C. (1973). *Fourier Transforms and their Physical Applications*. Academic Press, New York.

Feit, D. and Junger, M. C. (1969). High-frequency response of an elastic spherical shell. *J. Appl. Mech.* **36**, 859–864.
Fender, W. C. (1972). Scattering from an elastic spherical shell. Naval Undersea Center (currently Naval Ocean Systems Center) Tech. Report NUC-TR-313, San Diego, CA.
Friedlander, F. G. (1958). *Sound Pulses*. Cambridge University Press, Cambridge.
Gaunaurd, G. C. (1987). Techniques for sonar target-identification. *IEEE J. Ocean. Engng* **OE-12** (Special Issue on Scattering), 419–422.
Gaunaurd, G. C. (1989). Elastic and acoustic resonance wave scattering. *Appl. Mech. Rev.* **42**, 143–192, ASME Book No. AMR-056.
Gaunaurd, G. C. (1990). Distortions in the backscattering cross-sections of a submerged elastic shell due to its proximity to the sea surface or bottom. In *Computational Acoustics* (Edited by D. Lee *et al.*), Vol. 2, pp. 25–37. Elsevier, Amsterdam.
Gaunaurd, G. C. and Kalnins, A. (1982). Resonances in the sonar cross-sections of (coated) spherical shells. *Int. J. Solids Structures* **22**, 1149–1159.
Gaunaurd, G. C. and Tsui, C. Y. (1988). Transient and steady-state target resonance excitation by sound scattering. *Appl. Acoust.* **23**, 121–140.
Gaunaurd, G. C. and Ueberal, H. M. (1985). Relation between creeping-wave acoustic transients and the complex-frequency poles of the singularity expansion method. *J. Acoust. Soc. Am.* **78**, 234–243 (eqn 18).
Gaunaurd, G. C. and Werby, M. F. (1986). Proper background choice in resonance scattering by elastic shells. *Int. J. Solids Structures* **22**, 1149–1159.
Gaunaurd, G. C. and Werby, M. F. (1987). Lamb and creeping-wave around submerged spherical shells resonantly excited by sound scattering. *J. Acoust. Soc. Am.* **82**, 2021–2033.
Goodman, R. and Stern, R. (1962). Reflection and transmission of sound by an elastic spherical shell. *J. Acoust. Soc. Am.* **34**, 338–344.
Hickling, R. (1964). Analysis of echoes from a hollow metallic sphere in water. *J. Acoust. Soc. Am.* **36**, 1124–1137.
Junger, M. C. (1951). Sound scattering by thin elastic shells. *J. Acoust. Soc. Am.* **24**, 366.
Junger, M. C. and Feit, D. (1969). High-frequency response of point-excited submerged spherical shells. *J. Acoust. Soc. Am.* **45**, 630–636.
Junger, M. C. and Feit, D. (1972). *Sound, Structures and Their Interaction*. MIT Press, Cambridge, MA.
Kennaugh, E. M. and Cosgriff, R. L. (1958). The use of impulse response in electromagnetic scattering problems. *1958 IRE National Conv. Rec.*, Part 1, 72–77.
Kennaugh, E. M. and Moffatt, D. L. (1965). Transient and impulse response approximations. *Proc. IEEE* **53**, 893–901 (and references therein).
Kraus, H. and Kalnins, A. (1965). Transient vibrations of thin elastic shells. *J. Acoust. Soc. Am.* **38**, 994–1002.
Metsaveer, Y. A., *et al.* (1979). *Diffraction of Acoustic Pulses by Elastic Bodies*. Acd. Sci. Est. S.S.R., Valgus Publishing House, Tallinn [in Russian]. English translation by Wright-Patterson AFB, Ohio, FTD-ED (RS) T-1530-82 of Jan. 11, 1983.
Nigul, V. K. (1974). *Echo Signals from Elastic Objects*. Acad. Sci. Est. S.S.R., Valgus Publishing House, Tallinn [in Russian] (2 Vols). Translated by NISC-62, No. 6271, Washington, DC of 1975 (Vol. 2) and 1980 (Vol. 1).
Press, W. *et al.* (1986) *Numerical Recipes*, Chapter 12, pp. 390–429. Cambridge University Press, Cambridge.
Sergeev, A. V. (1985). Determination of the parameters of a spherical elastic shell from the scattered wave-field. *Soviet Phys. Acoust.* **31**, 55–58.
Strifors, H. and Gaunaurd, G. (1989). Transient scattering of sound pulses by underwater viscoelastic bodies. *Proc. First Pan American Congress of Applied Mechanics (PACAM)*, PUC, Brasil, pp. 756–760.
Tsui, C. Y., *et al.* (1988). Bistatic measurements of target scattering at resonance. *J. Acoust. Soc. Am.* **83**, 1946–1951.
Ueberal, H. M. and Gaunaurd, G. C. (1984). Relation between the ringing of resonances and surface waves in radar scattering. *IEEE Trans.* **AP-32**, 1071–1079 (eqn 20).
Veksler, N. (1982). *Information Analysis in Hydroelasticity*. Acad. Sci. Est. S.S.R., Valgus Publishing House, Tallinn [in Russian]. English translation by NISC-62, No. 9047 of Feb. 8, 1983.
Veksler, N. (1984). *Resonansnoye Rasseyaniye v gidroakustike*. Acad. Sci. Est. S.S.R., Valgus Publishing House, Tallinn [in Russian].
Werby, M. F. (1989). Time-domain solution from the frequency domain: application to resonance scattering from elastic bodies. *Proc. 2nd IMACS Conf. on Computational Acoustics*, Princeton, NJ, pp. 320–350. North-Holland, Amsterdam.
Weyker, R. and Dudley, D. (1987). Identification of resonances of an acoustically rigid sphere. *IEEE J. Ocean. Engng* **OE-12** (Special Issue on Scattering), 317–326.

APPENDIX

The elements d_{ij} of the determinants in eqn (4) were all given in Ayres *et al.* (1987). A few typos/misprints appeared in five of these elements, namely d_{21}, d_{41}, d_{44}, d_{64} and d_{65}. To set the record straight we give the corrected forms below:

$$d_{21} = k_1 a h_n^{(1)\prime}(k_1 a)$$

$$d_{41} = 4k_{t2} b y_n'(k_{t2} b) + [2n(n+1) - k_{t2}^2 b^2] y_n(k_{t2} b)$$

$$d_{44} = 2n(n+1)[k_{t2} b j_n'(k_{t2} b) - j_n(k_{t2} b)]$$

$$d_{64} = 2k_{t2} b j_n'(k_{t2} b) + [k_{t2}^2 b^2 - 2n(n+1) + 2] j_n(k_{t2} b)$$

$$d_{65} = 2k_{t2} b y_n'(k_{t2} b) + [k_{t2}^2 b^2 - 2n(n+1) + 2] y_n(k_{t2} b).$$

The underlined letters correct the earlier errors.